Low-lying excitations of double Bose-Einstein condensates

B. D. Esry and Chris H. Greene
Department of Physics and JILA, University of Colorado, Boulder, Colorado 80309-0440
(Received 11 July 1997)

We present the excitation spectrum of a double Bose-Einstein condensate for the JILA time orbiting potential trap including the effects of gravity. We consider two cases: (i) fixed scattering lengths and equal numbers of each atomic species as a function of the number of atoms and (ii) fixed intraspecies scattering lengths and a fixed, equal number of atoms in each state as a function of interspecies scattering length. The spectra reveal the rich dynamics of the system and in particular show simultaneous collective excitations of both condensates. [S1050-2947(98)06302-1]

PACS number(s): 03.75.Fi, 05.30.Jp

I. INTRODUCTION

In the two years since the initial achievement of Bose-Einstein condensation in a dilute atomic gas [1], three groups have repeated the feat [2–4] and several quantitative studies have been completed [5–9]. In the course of those two years an exciting possibility was also serendipitously discovered: the ability to simultaneously trap and condense two different atomic species [4]. An especially promising result of this discovery is the possibility of sympathetically cooling an atomic species to the point of condensation that would otherwise be prohibitively difficult to accomplish directly. Experiments on double Bose-Einstein condensates have not yet progressed beyond creation and observation, but hopefully can soon produce the quantitative results that have characterized recent single-condensate experiments.

Compared to single condensates, little theoretical work has been carried out for realistic double condensates, although both the ground state and excited states have been studied in the Hartree-Fock [10] and Thomas-Fermi [11,12] approximations for model systems. The primary effect neglected in these models is the displacement of the minimum of the effective harmonic trapping potential, which is generally different for each atomic species, due to the atoms' gravitational energy. One calculation [13], however, has included this effect for an experimentally realistic geometry, but considered only the ground state. In this paper we extend that study of the double condensate ground state to a time orbiting potential (TOP) trap configuration and consider greater variations in the parameters. We study the TOP trap rather than the baseball trap configuration in which the double condensate has been observed because even with the gravitational shift of the effective trapping potential for each species, the system possesses cylindrical symmetry. The geometry of the double condensate in the TOP trap can be visualized as two pancakes lying on top of one another, whereas the picture for the experiment of Myatt *et al.* resembles two parallel, horizontal cigars, one of which lies on top of the other. The TOP trap computation can thus be reduced to two dimensions, which greatly facilitates exploration of various parameter combinations. In addition, the results retain direct physical relevance to experiment.

One of the intriguing properties of double condensates is the simultaneous excitation of collective modes of both species. To probe these dynamics, we have calculated the excitation spectrum of the TOP trap double condensate for a wide range of parameters. We find a rich excitation spectrum, with states for which both condensates respond equally to the driving field. There are also states, however, for which one condensate responds much more strongly than the other. With the use of nondestructive imaging techniques, it is entirely feasible that both types of excitations will be observed experimentally in real time.

The Hartree-Fock and random-phase approximation equations for the double condensate are developed in Sec. II, while Sec. III discusses our results for the TOP trap. We summarize in Sec. IV.

II. THEORY

We briefly outline the derivation of the Hartree-Fock and the random-phase approximation (RPA) equations for the double-condensate system, following closely the development in Ref. [14] for single condensates. We make the independent-particle approximation and assume that the number of atoms N_1 and N_2 in each species is separately conserved. The states of the system are then described in terms of symmetrized products of the single-particle states $\{\psi_i\}$ and $\{\phi_j\}$ for each species, respectively. The Hamiltonian can then be written as

$$\hat{H}=\hat{H}_1+\hat{H}_2+\hat{V}_{12}, \tag{1}$$

where $\hat{H}_1$ and $\hat{H}_2$ are the intraspecies Hamiltonians and $\hat{V}_{12}$ is the interspecies interaction term. Explicitly, in second-quantized form

$$\hat{H}_1=\sum_{\alpha,\beta}\hat{c}_\alpha^\dagger\langle\psi_\alpha|h_1|\psi_\beta\rangle\hat{c}_\beta + \frac{1}{2}\sum_{\alpha,\beta,\gamma,\delta}\hat{c}_\alpha^\dagger\hat{c}_\beta^\dagger\langle\psi_\alpha\psi_\beta|V_{11}|\psi_\gamma\psi_\delta\rangle\hat{c}_\delta\hat{c}_\gamma,$$

$$\hat{H}_2=\sum_{\alpha,\beta}\hat{d}_\alpha^\dagger\langle\phi_\alpha|h_2|\phi_\beta\rangle\hat{d}_\beta + \frac{1}{2}\sum_{\alpha,\beta,\gamma,\delta}\hat{d}_\alpha^\dagger\hat{d}_\beta^\dagger\langle\phi_\alpha\phi_\beta|V_{22}|\phi_\gamma\phi_\delta\rangle\hat{d}_\delta\hat{d}_\gamma, \tag{2}$$

where

$$h_i = -\frac{\hbar^2}{2m_i}\nabla^2 + \frac{1}{2}m_i[\omega_{ix}^2 x^2 + \omega_{iy}^2 y^2 + \omega_{iz}^2 (z - z_{i0})^2].$$

In this expression, m_i is the mass of the ith species atom, $\omega_{i\alpha}$ is the trap frequency along axis α for the ith species ($\omega_{ix} = \omega_{iy} = \omega_{i\rho}$, $\omega_{iz} = \sqrt{8}\omega_{i\rho}$, and $\omega_{2\alpha} = \sqrt{2}\omega_{1\alpha}$ for trapping the $|F=1, M_F=-1\rangle$ and $|2,2\rangle$ hyperfine states of ^{87}Rb in the TOP trap), and $z_{i0} = -g/\omega_{iz}^2$ is the displacement of the ith trap center due to the gravitational acceleration g. The creation and annihilation operators $\hat{c}$ and $\hat{d}$ for each species are defined in terms of their effect on a number state of the system. That is, $\hat{c}_\alpha^\dagger$ ($\hat{c}_\alpha$) creates (annihilates) an atom of species 1 in the state ψ_α with the prefactor $\sqrt{n_\alpha + 1}$ ($\sqrt{n_\alpha}$) while leaving all atoms of species 2 unaffected; $\hat{d}_\beta^\dagger$ ($\hat{d}_\beta$) is the analogous operator for species 2. The operators $\hat{c}$ and $\hat{d}$ obey boson commutation relations $[\hat{c}_\alpha, \hat{c}_\beta^\dagger] = [\hat{d}_\alpha, \hat{d}_\beta^\dagger] = \delta_{\alpha\beta}$ with all other commutators, including the mixed commutators of $\hat{c}$ and $\hat{d}$, equal to zero.

For indistinguishable atoms, the interspecies interaction term is given by

$$\hat{V}_{12} = \sum_{\alpha,\beta,\gamma,\delta} \hat{c}_\alpha^\dagger \hat{d}_\beta^\dagger \langle \psi_\alpha \phi_\beta | \overline{V_{12}} | \psi_\gamma \phi_\delta \rangle \hat{c}_\delta \hat{d}_\gamma \tag{3}$$

using the shorthand notation

$$\langle \psi_\alpha \phi_\beta | \overline{V_{12}} | \psi_\gamma \phi_\delta \rangle = \langle \psi_\alpha \phi_\beta | V_{12} | \psi_\gamma \phi_\delta \rangle + \langle \psi_\alpha \phi_\beta | V_{12} | \phi_\delta \psi_\gamma \rangle \tag{4}$$

for the direct and exchange contributions. Note that this interaction differs from the intraspecies interaction terms in Eq. (2) by a factor of 1/2. This factor is not needed since there is no double counting in the sum over all α and β, i.e., $\hat{c}_\alpha^\dagger \hat{d}_\beta^\dagger \neq \hat{c}_\beta^\dagger \hat{d}_\alpha^\dagger$. Additionally, because this symmetry under index exchange is absent, the direct and exchange terms must be explicitly built into the interspecies interaction.

For distinguishable atoms, the construction of direct and exchange matrix elements is of course not relevant. Thus the matrix element in Eq. (3) is replaced by the unsymmetrized version

$$\langle \psi_\alpha \phi_\beta | \overline{V_{12}} | \psi_\gamma \phi_\delta \rangle \rightarrow \langle \psi_\alpha \phi_\beta | V_{12} | \psi_\gamma \phi_\delta \rangle.$$

We approximate all interatomic interactions V_{ij} by a Dirac δ-function pseudopotential, $V_{ij} = U_{ij}\delta(r_{ij})$, whose coefficient is given by

$$U_{ij} = \frac{2\pi\hbar^2 a_{ij}}{\mu_{ij}},$$

where a_{ij} is the s-wave scattering length between an i species atom and a j species atom and $\mu_{ij} = m_i m_j/(m_i + m_j)$ is the reduced mass. The justification for this approximation has been discussed previously [14,15], although its validity has been more rigorously examined recently by Proukakis, Burnett, and Stoof [16]. In this approximation, the interaction matrix elements reduce to

$$\langle \psi_\alpha \psi_\beta | V_{ij} | \psi_\gamma \psi_\delta \rangle = U_{ij} \int d^3x \, \psi_\alpha^*(\mathbf{x}) \psi_\beta^*(\mathbf{x}) \psi_\gamma(\mathbf{x}) \psi_\delta(\mathbf{x}) \tag{5}$$

save for the indistinguishable case (4), which instead is

$$\langle \psi_\alpha \phi_\beta | \overline{V_{12}} | \psi_\gamma \phi_\delta \rangle = U_{12} \int d^3x \, \psi_\alpha^*(\mathbf{x}) \phi_\beta^*(\mathbf{x}) \psi_\gamma(\mathbf{x}) \phi_\delta(\mathbf{x}).$$

The Hartree-Fock equations are obtained by minimizing the total energy with respect to the orbitals ψ_0^* and ϕ_0^*,

$$\frac{\delta}{\delta\psi_0^*}\langle N_1; N_2 | \hat{H} | N_1; N_2 \rangle = 0, \quad \frac{\delta}{\delta\phi_0^*}\langle N_1; N_2 | \hat{H} | N_1; N_2 \rangle = 0.$$

The minimization is constrained by requiring ψ_0^* and ϕ_0^* to be normalized to unity. Orthogonality is generally ensured by the orthogonality of the spin states. The equations for ψ_n and ϕ_n are then

$$[h_1 + (N_1 - 1)U_{11}|\psi_0|^2 + N_2 U_{12}|\phi_0|^2]\psi_n = \varepsilon_{1n}\psi_n,$$

$$[h_2 + N_1 U_{12}|\psi_0|^2 + (N_2 - 1)U_{22}|\phi_0|^2]\phi_n = \varepsilon_{2n}\phi_n. \tag{6}$$

For $n = 0$, these are coupled nonlinear (or self-consistent) equations for ψ_0 and ϕ_0, while for $n > 0$ they are uncoupled linear equations for the single-particle basis states $\{\psi_i\}$ and $\{\phi_j\}$. Their structure is very similar to the Hartree-Fock (or Gross-Pitaevskii or nonlinear Schrödinger) equation for a single condensate and up to possible factors of 2 [13] are a relatively straightforward generalization of the single-condensate result. It should be noted that this is not the only choice for the single-particle basis, but it is convenient and includes much of the mean-field effects due to the condensate.

The energies determined from Eq. (6) yield an approximate single-particle excitation spectrum of the condensate. In general, however, this approximation will be quite poor [14]. An improved spectrum can be obtained using the RPA, which for single condensates has proven successful in describing experimentally measured zero-temperature excitation energies [14,17]. The RPA has been shown to be largely equivalent to the Bogoliubov approximation [14,18] and to give essentially the same numerical results [14]. The RPA is based upon determining an operator $\hat{O}^\dagger$ such that approximate excited states of the system can be determined from

$$\hat{O}_\nu^\dagger |\Phi_0^{\mathrm{RPA}}\rangle = |\Phi_\nu^{\mathrm{RPA}}\rangle,$$

where $|\Phi_0^{\mathrm{RPA}}\rangle$ is the RPA approximation to the exact ground state of the system. The heart of the RPA approximation lies in limiting the operator $\hat{O}$ to include only single-particle excitations. If one makes the further ''quasiboson approximation'' in which the RPA ground state is replaced by the Hartree-Fock ground state $|N_1; N_2\rangle$, then the operators $\hat{O}$ can be written in terms of another set of operators defined as

$$\hat{C}_p^\dagger = \frac{\hat{c}_p^\dagger \hat{c}_0}{\sqrt{N_1}}, \quad \hat{D}_p^\dagger = \frac{\hat{d}_p^\dagger \hat{d}_0}{\sqrt{N_2}}.$$

To approximately order N_i^{-1}, these operators also satisfy boson commutation relations [14]. Physically, they create single-particle excitations from the Hartree-Fock ground state in one or the other of the atomic species. The explicit form for the operator $\hat{O}_\nu^\dagger$ in terms of these operators is

$$\hat{O}_\nu^\dagger=\sum_{p\neq 0} X_{p\nu}\hat{C}_p^\dagger - Y_{p\nu}\hat{C}_p + \sum_{p\neq 0} U_{p\nu}\hat{D}_p^\dagger - V_{p\nu}\hat{D}_p .$$

It must be remembered that the index p in the first sum refers to the single-particle orbitals $\{\psi_i\}$, while in the second sum p refers to the set $\{\phi_j\}$. Requiring the $\hat{O}_\nu$ to also satisfy boson commutation relations leads to the orthonormality condition

$$\sum_{p\neq 0} X_{p\nu'}^* X_{p\nu} - Y_{p\nu'}^* Y_{p\nu} + \sum_{p\neq 0} U_{p\nu'}^* U_{p\nu} - V_{p\nu'}^* V_{p\nu} = \delta_{\nu'\nu}.$$

The quasiboson RPA to the excited-state energy of the entire system can thus be written as

$$E_\nu - E_0 = \frac{\langle N_1;N_2|[\hat{O}_\nu,[\hat{H},\hat{O}_\nu^\dagger]]|N_1;N_2\rangle}{\langle N_1;N_2|[\hat{O}_\nu,\hat{O}_\nu^\dagger]|N_1;N_2\rangle}. \tag{7}$$

The equations for X, Y, U, and V are derived by taking variations of Eq. (7) with respect to their complex conjugates. Since approximations have been made in deriving Eq. (7), however, the energies obtained are not Rayleigh-Ritz variational approximations to the exact energies of the system. Defining the coefficient matrices

$$L_{qp}=\frac{N_1-1}{2\hbar}\langle\psi_q\psi_0|\overline{V_{11}}|\psi_p\psi_0\rangle,$$

$$M_{qp}=\frac{N_2-1}{2\hbar}\langle\phi_q\phi_0|\overline{V_{22}}|\phi_p\phi_0\rangle,$$

$$N_{qp}=\frac{\sqrt{N_1N_2}}{\hbar}\langle\psi_q\phi_0|\overline{V_{12}}|\psi_0\phi_p\rangle$$

and recalling the simplification afforded by the pseudopotential approximation (5), the RPA equations for the double-condensate system can be summarized in matrix form as

$$\begin{pmatrix} \Omega_1+\mathbf{L} & \mathbf{L} & \mathbf{N} & \mathbf{N} \\ \mathbf{L} & \Omega_1+\mathbf{L} & \mathbf{N} & \mathbf{N} \\ \mathbf{N}^T & \mathbf{N}^T & \Omega_2+\mathbf{M} & \mathbf{M} \\ \mathbf{N}^T & \mathbf{N}^T & \mathbf{M} & \Omega_2+\mathbf{M} \end{pmatrix} \begin{pmatrix} X_\nu \\ Y_\nu \\ U_\nu \\ V_\nu \end{pmatrix} = \omega_\nu \begin{pmatrix} X_\nu \\ -Y_\nu \\ U_\nu \\ -V_\nu \end{pmatrix}. \tag{8}$$

The entries of the diagonal matrices Ω_i are just the excitation energies of the basis states, $\hbar\Omega_{iq}=\varepsilon_{iq}-\varepsilon_{i0}$, and $\hbar\omega_\nu=E_\nu-E_0$ is the excitation energy of the system as a whole. In the limit $\mathbf{N}\to 0$ ($a_{12}\to 0$), these equations reduce to single-condensate RPA equations for each species [14].

III. RESULTS AND DISCUSSION

We have solved both the Hartree-Fock equations (6) and the RPA equations (8) for a wide range of parameters relevant to trapping the $|1,-1\rangle$ and $|2,2\rangle$ hyperfine states of ^{87}Rb in the JILA TOP trap. Throughout the remainder of this article we will use the notation $|1\rangle\equiv|1,-1\rangle$ and $|2\rangle\equiv|2,2\rangle$. As a practical experimental matter, excitations of a double condensate can be measured just as for single condensates. That is, one can perturb the trapping potential by adding a harmonic driving field of the appropriate symmetry to reach the desired final state. The effective trapping potential for both species will be modulated at the same frequency and the density of one or both of the species [4] can then be observed as a function of time [5,6]. It may turn out, however, that one species or the other can respond with a larger amplitude for a given excitation frequency, a situation we discuss in more detail below.

In a given trap, the ground and excited states of single condensates can be characterized by a one-parameter encompassing particle number, scattering length, and one of the trap frequencies. In the same trap, the five parameters for a double condensate, the number of atoms of each species plus the three scattering lengths, cannot similarly be reduced to such a useful parameter (or set of parameters). This makes general properties more difficult to ascertain, but it also allows much richer possibilities for the dynamics of both the ground and excited states. We have explored a small portion of this parameter space, calculating spectra for two cases: (i) fixed scattering lengths and equal numbers in each hyperfine state as a function of the number of particles and (ii) fixed intraspecies scattering lengths and a fixed, equal number of atoms in each state as a function of interspecies scattering length. For both cases, we chose $\omega_{2\rho}=2\pi\times 133$ Hz, which gives for the displacements of the effective harmonic trapping potentials $z_{10}=-3.51$ μm and $z_{20}=-1.75$ μm.

A. Atom number dependence

In the first case we considered, we fixed the scattering lengths at their physical values for the $|2,2\rangle$ and $|1,-1\rangle$ hyperfine states of ^{87}Rb. From Burke *et al.* [19] (see also [20,21]), these are $a_{11}=108.8$ a.u., $a_{22}=109.1$ a.u., and $a_{12}=108.0$ a.u. In addition, the numbers of atoms in each species were taken to be equal $N_1=N_2=N$, as was approximately the case experimentally [4]. We have previously discussed the properties of the ground state for this case in Ref. [13] for the parameters of the Myatt *et al.* experiment and find no significant qualitative differences for the TOP trap aside from its different geometry. Consequently, our discussion here concentrates on the excited-state properties.

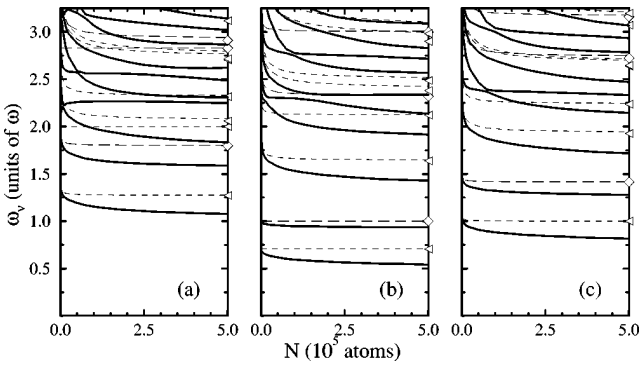

FIG. 1. RPA excitation frequencies as a function of $N=N_1=N_2$ for $a_{11}=108.8$ a.u., $a_{22}=109.1$ a.u., and $a_{12}=108.0$ a.u. [19]: (a) $M=0$, (b) $M=1$, and (c) $M=2$. The coupled condensate frequencies are indicated by the heavy solid lines, while the uncoupled frequencies are indicated by the thin dashed and long-dashed lines for the $|1,-1\rangle$ and $|2,2\rangle$ states, respectively. The symbols at the right hand side of each plot indicate the frequencies in the hydrodynamic limit [23]: triangles for $|1,-1\rangle$ and diamonds for $|2,2\rangle$.

Because the TOP trap retains cylindrical symmetry even for the double-condensate system, the projection of the total angular momentum on the symmetry axis M is a good quantum number. In Fig. 1 we show several of the lowest RPA excitation frequencies for $M=0,1$, and 2 with the frequency axis scaled by $\omega_{2\rho}=2\pi\times 133$ Hz. To aid in the classification of the states and to show the effects of the interaction of the two condensates we include in the figure the RPA excitation frequencies for uncoupled condensates $a_{12}=0$. We note that the excitation frequencies differ significantly from the uncoupled frequencies for essentially all of the states shown. We also note that the uncoupled frequencies for the largest number of atoms reported here, $N=500\,000$, agree well with the analytical results available in the hydrodynamic limit [22,23]. For some of the higher-lying excitations though, it appears that the hydrodynamic limit has not yet been reached by $N=500\,000$ with the numerical frequencies being up to about 5% higher than the analytical frequencies. The numerical results are, however, uncertain to within a few percent due to basis-set truncation of the RPA equations, making a definitive statement difficult.

It happens that $\omega_{1z}=\omega_{2\rho}$ and $2\omega_{1\rho}=\omega_{2z}$ for the $|1,-1\rangle$ and $|2,2\rangle$ hyperfine states in the TOP trap. These ''accidentally'' commensurate frequencies appear ideal for simultaneous collective modes of both species due to the possibility of resonant energy transfer between the condensates. The mean field, however, quickly removes this degeneracy, thus mitigating it as a mechanism for the generation of simultaneous modes.

The lowest two frequencies for each M in Fig. 1 are primarily due to the response of one or the other of the atomic species. That this is the case can be seen more clearly by considering oscillations in the expectation value of the number density for the singly excited time-dependent wave function

$$|\Psi(t)\rangle=\alpha|N_1;N_2\rangle+\beta e^{-i\omega_\nu t}|\Phi_\nu^{\mathrm{RPA}}\rangle.$$

This form of the wave function applies, for instance, after some period of driving the condensate, although it will more

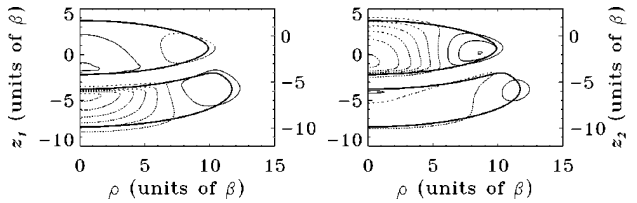

FIG. 2. Density oscillation [see Eq. (9)] for the lowest two excitations with $N_1=N_2=5\times10^5$, $a_{11}=108.8$ a.u., $a_{22}=109.1$ a.u., and $a_{12}=108.0$ a.u.: (a) $\nu=1$ and (b) $\nu=2$. The contours are evenly spaced with negative values indicated by dotted lines and positive by solid lines. The heavy solid line marks the extent of the ground state at the level of the lowest positive contour (see Fig. 3). Note that the z axis has been shifted for the upper ($|2,2\rangle$) state according to the right-hand axes. With $\omega_{2\rho}=2\pi\times133$ Hz, $\beta=\sqrt{\hbar/m\omega}=0.935$ μm.

generally also have multiply excited-state contributions. The observable most often measured experimentally is the number density, and for double condensates the number density of each species can be measured separately. Thus one revealing quantity is the expectation value of the species specific number density operator

$$\hat{n}_1(\mathbf{x})=\sum_{\alpha,\beta}\hat{c}_\alpha^\dagger\hat{c}_\beta\psi_\alpha^*(\mathbf{x})\psi_\beta(\mathbf{x})$$

[$\hat{n}_2(\mathbf{x})$ has the same form with $\hat{c}\to\hat{d}$ and $\psi\to\phi$]. Experimentally, the total number density can also be measured, while theoretically it is calculated as the expectation value of $\hat{n}=\hat{n}_1+\hat{n}_2$. For the above wave function, the expectation value is thus

$$\begin{aligned}\langle\Psi(t)|\hat{n}_1(\mathbf{x})|\Psi(t)\rangle&=|\alpha|^2\langle N_1;N_2|\hat{n}_1(\mathbf{x})|N_1;N_2\rangle+|\beta|^2\langle\Phi_\nu^{\mathrm{RPA}}|\hat{n}_1(\mathbf{x})|\Phi_\nu^{\mathrm{RPA}}\rangle\\&\quad+2\,\mathrm{Re}[\alpha^*\beta e^{-i\omega_\nu t}\langle N_1;N_2|\hat{n}_1(\mathbf{x})|\Phi_\nu^{\mathrm{RPA}}\rangle].\end{aligned}$$

Since the oscillation in the experimentally measured width is entirely due to the cross term in this expression (and to its analogy when multiple excitations are present), the quantity

$$\Delta\langle\hat{n}_i(\mathbf{x})\rangle=\langle N_1;N_2|\hat{n}_i(\mathbf{x})|\Phi_\nu^{\mathrm{RPA}}\rangle,\quad i=1,2,\qquad(9)$$

provides a convenient way to visualize the qualitative behavior of a given excited state. We show in Fig. 2 the density

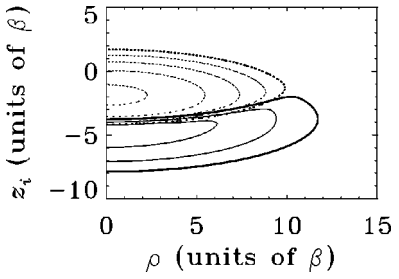

FIG. 3. Ground-state density for $N_1=N_2=5\times10^5$, $a_{11}=108.8$ a.u., $a_{22}=109.1$ a.u., and $a_{12}=108.0$ a.u. The solid line corresponds to the $|1,-1\rangle$ state and the dotted to $|2,2\rangle$. The heavy lines are identical to those in Figs. 2 and 4. With $\omega_{2\rho}=2\pi\times133$ Hz, $\beta=\sqrt{\hbar/m\omega}=0.935$ μm.

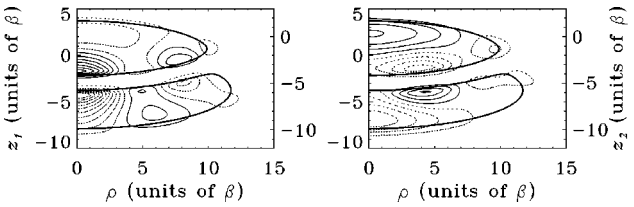

FIG. 4. Density oscillation [see Eq. (9)] for $N_1=N_2=5\times10^5$, $a_{11}=108.8$ a.u., $a_{22}=109.1$ a.u., and $a_{12}=108.0$ a.u.: (a) $\nu=6$ and (b) $\nu=7$. The contours are evenly spaced with negative values indicated by dotted lines and positive by solid lines. The heavy solid line marks the extent of the ground state at the level of the lowest positive contour (see Fig. 3). Note that the z axis has been shifted for the upper ($|2,2\rangle$) state according to the right-hand axes. With $\omega_{2\rho}=2\pi\times133$ Hz, $\beta=\sqrt{\hbar/m\omega}=0.935$ μm.

oscillation (9) weighted by $\sqrt{N_i}$ for each species, for the two lowest $M=0$ states. It is plotted in the ρ-z plane with the z axis of the $|2,2\rangle$ state (the upper condensate in the figure) shifted upward (to make each separate condensate more clearly visible in the figure) according to the axis on the right-hand side of the plot. Unshifted, the two overlap by about one-half oscillator unit along the entire length of their interface as can be seen in the ground-state number density in Fig. 3. In both figures, the contours are equally spaced and the heavy contours indicate the extent of the ground state at the level of the lowest positive contour. In Fig. 2(a), it can be seen that the $|1,-1\rangle$ state (the lower condensate in the figure) is responding much more strongly than the $|2,2\rangle$ state and in Fig. 2(b) just the opposite can be seen. The same is true to about the same degree for the lowest two excitations of both the $M=1$ and $M=2$ symmetries. Because of the distribution of negative and positive density oscillations (these are the dotted and solid contours in Fig. 2, respectively), excitations of the lowest two states are seen to cause oscillations of the clouds that are almost entirely radial.

Higher in the spectra in Fig. 1 several avoided crossings can be seen as the excitations that are primarily in the z direction get pushed higher with increasing N by the larger mean field. At $N\rightarrow1$ the third excited state, for instance, converges to the $(n_{1\rho},n_{1z};n_{2\rho},n_{2z})=(0,1;0,0)$ harmonic-oscillator state. As N increases, its excitation frequency rapidly increases until it reaches an avoided crossing with the state with $(n_{1\rho},n_{1z};n_{2\rho},n_{2z})=(2,0;0,0)$ character. After the crossing, the third excited state is mostly this ρ excitation, while the fourth excited state carries the n_{1z} excitation. Finally, at $N=500\,000$, the fourth excited state is mostly $(n_{1\rho},n_{1z};n_{2\rho},n_{2z})=(0,1;1,0)$ in character with a large admixture of $(n_{1\rho},n_{1z})=(1,0)$, where the quantum numbers $n_{i\rho}$ and n_{iz} now count nodes along each coordinate for the nonseparable Hartree-Fock wave functions. It is useful at this point to recall the stacked pancake geometry of the TOP trap in which the z axis is the symmetry axis of the system. The higher energetic cost for excitations along this direction as N increases is physically reasonable since each condensate sees an increasingly hard wall due to the mean field of the other condensate. On the other hand, the trend for the excitations in the radial direction is just the opposite. Again, this is physically reasonable since the condensates grow larger in this dimension as N increases, thus increasing the longest wavelength supported by the system. This is especially true

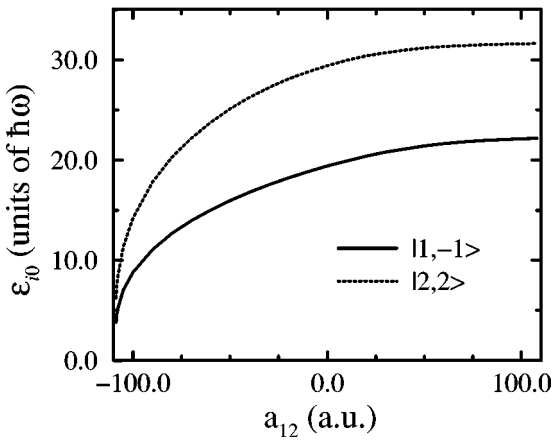

FIG. 5. Ground orbital energies for $N_1=N_2=10^5$, $a_{11}=108.8$ a.u., and $a_{22}=109.1$ a.u. as a function of interspecies scattering length. The solid line corresponds to the $|1,-1\rangle$ state and the dotted to $|2,2\rangle$.

for the $|1,-1\rangle$ condensate as it tends to lengthen by wrapping around the $|2,2\rangle$ condensate. The state that corresponds to the $(n_{1\rho},n_{1z};n_{2\rho},n_{2z})=(3,0;0,0)$ harmonic-oscillator state with an excitation energy of $4.2\hbar\omega_{2\rho}$, for example, drops from the ninth excited state at $N=1$ to the fifth at $N=500\,000$ with an excitation frequency of $\omega_5=2.3\omega_{2\rho}$. For the uncoupled condensates, it drops to only the seventh excited state (counting both condensates) with an excitation frequency of $\omega_7=2.8\omega_{2\rho}$.

Nearly all of the states above $\nu=2$ exhibit a simultaneous response of both condensates to driving. The ratio of the peak amplitudes for each ranges from about 2 to unity. The more interesting case of approximately equal response is exhibited in Fig. 4. The sixth and seventh excited $M=0$ states are shown; similar examples could be drawn from both the $M=1$ and $M=2$ symmetries. For $\nu=6$ [Fig. 4(a)] the radial and axial motions are coupled, albeit weakly, in a manner such that the total time-dependent density appears to transfer from the $|2,2\rangle$ state to the $|1,-1\rangle$ state along z and to a lesser extent along ρ for each. For $\nu=7$ [Fig. 4(b)], the coupling of radial and axial motions is stronger. This suggests that the density sloshes in phase along z for both species while also expanding and contracting in ρ.

B. Interspecies scattering length dependence

In the second case considered, we fixed the number of atoms in each species to be $N_1=N_2=10^5$ and the scattering lengths a_{11} and a_{22} to be 108.8 a.u. and 109.1 a.u., respectively, and left the interspecies scattering length a_{12} free to vary. This might not be easily realized experimentally for the present choice of atomic species, but will almost certainly be attainable for some combination of atoms. It is likely, in fact, that the entire range of interspecies scattering length values could be explored by tuning the molecular interaction potentials with an external field [24,25]. One promising combination is the mixed isotope system ^{85}Rb+^{87}Rb in the lower trapped hyperfine states $|2,-2\rangle$ and $|1,-1\rangle$ states, respectively [26]. In Ref. [13] we briefly discussed some of the ground-state properties as a function of a_{12} for the Myatt *et al.* experiment [4]. Here we expand on that discussion, fo-

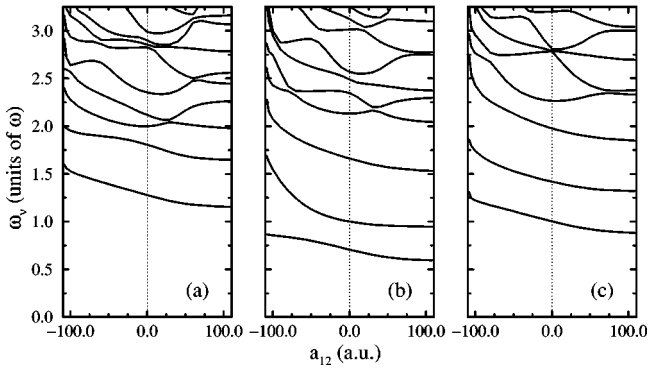

FIG. 6. RPA excitation frequencies as a function of a_{12} (in a.u.) with $a_{11}=108.8$ a.u., $a_{22}=109.1$ a.u., and $N_1=N_2=10^5$: (a) $M=0$, (b) $M=1$, and (c) $M=2$.

cusing on the TOP trap geometry. We show in Fig. 5 the ground-state orbital energies. It can be seen that $a_{12}\approx -110$ a.u. is a critical point at which the orbital energies grow rapidly smaller. In the Thomas-Fermi approximation, double condensates with $a_{12}\leqslant -a_{12}^c=-\sqrt{a_{11}a_{22}}$ are, in fact, unstable (in the present case $a_{12}^c=109.0$ a.u.). Ground-state instabilities are typically expected to appear in the RPA excitation spectrum as an excitation frequency that becomes identically zero for some value of a parameter a_{12}, for example [27–29]. Such behavior was explicitly shown by Dodd *et al.* [29] for a single condensate of ^{7}Li. From the excitation spectra in Fig. 6, however, we see that the excitation frequencies remain strictly positive with no tendancy towards zero at the critical value of the interspecies scattering length. It follows that the instability expected for the double condensate is not of the same character as for single condensates. While the Hartree-Fock approach shows the symptoms of breaking down, it does not provide for the remedy nor does it give a clear indication why. As a result, we are currently exploring these questions from a different perspective [30].

The qualitative behavior of the excitation frequencies as a function of a_{12} can be understood in terms of the change in the size of the condensate. As a_{12} increases from zero, the situation is essentially as described above for increasing N: The excitations in ρ decrease in frequency, while those in z increase. As a_{12} decreases from zero, though, the condensates are getting steadily smaller, forcing the excitation frequencies higher in energy for both ρ and z excitations. That this is the case can be seen in Fig. 6 with few exceptions. Generally, then, it follows that excitations predominantly in the z direction increase in frequency as $|a_{12}|$ increases, while excitations primarily in the ρ direction decrease as a_{12} increases from the value $-a_{12}^c$.

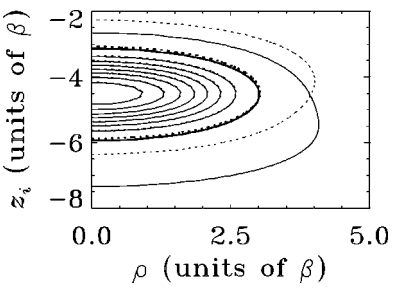

FIG. 7. Ground-state density for $N_1=N_2=10^5$, $a_{11}=108.8$ a.u., $a_{22}=109.1$ a.u., and $a_{12}=-108.0$ a.u. The solid line corresponds to the $|1,-1\rangle$ state and the dotted to $|2,2\rangle$. The heavy lines are identical to those in Fig. 8. With $\omega_{2\rho}=2\pi\times 133$ Hz, $\beta=\sqrt{\hbar/m\omega}=0.935$ μm.

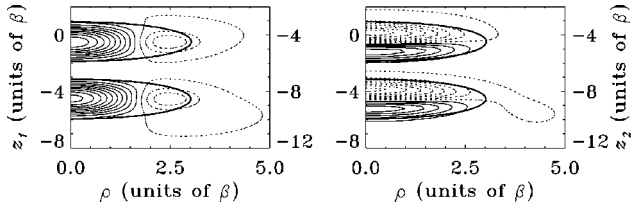

FIG. 8. Density oscillation [see Eq. (9)] for $N_1=N_2=5\times10^5$, $a_{11}=108.8$ a.u., $a_{22}=109.1$ a.u., and $a_{12}=-108.0$ a.u.: (a) $\nu=1$ and (b) $\nu=3$. The contours are evenly spaced with negative values indicated by dotted lines and positive by solid lines. The heavy solid line marks the extent of the ground state at the level of the lowest positive contour (see Fig. 7). Note that the z axis has been shifted for the upper $|2,2\rangle$ state according to the right-hand axes. With $\omega_{2\rho}=2\pi\times133$ Hz, $\beta=\sqrt{\hbar/m\omega}=0.935$ μm.

In Fig. 7 we show the ground state for $a_{12}=-108.0$ a.u. With an interspecies scattering length so large in magnitude, the mean field for one species due to the other becomes comparable to its own. The attraction is great enough, in fact, to overcome the gravitationally induced separation so that the condensates lie almost completely on top of one another. Note that each of the condensates are essentially the same above the first contour in Fig. 7. Furthermore, given that the uncoupled condensates are about $12\times4.5(\rho\times z)$ oscillator units full width at half maximum (FWHM) and 10×3.5 oscillator units for the $|1,-1\rangle$ and $|2,2\rangle$ states, respectively, the condensates in Fig. 7 are much smaller, in accord with the qualitative discussion above for the behavior of the excitation frequencies.

In Fig. 8 we show the density oscillations $\Delta\langle\hat{n}_i(\mathbf{x})\rangle$ for the first and third $M=0$ excited states corresponding to the ground state in Fig. 7. In this configuration, the two behave as essentially a single-species condensate. This is manifested in both Figs. 8(a) and 8(b) (the $|2,2\rangle$ state has been shifted upward as for Figs. 2 and 4; compare Fig. 7) since the amplitude and topology of each condensate's response matches almost completely. It is worth noting that even though the Hartree-Fock ground state is, in principle, stable for this value of a_{12}, the lifetime of the double condensate is normally severely shortened due to inelastic two- and three-body processes [13,19,20]. Unfortunately, it is likely that the lifetime is too short to make experimental observations possible for a_{12} so near $-a_{12}^c$. If such an experiment were possible, however, the density variations should still be measurable independently and would show purely radial breathing for the first excited state and purely axial sloshing for the third.

IV. SUMMARY

We have presented calculated RPA excitation spectra for a double condensate in a TOP trap exploring their dependence on the number of atoms and on the interspecies scattering length. Further, since the spatial distributions depend

on these parameters, we have shown that the excitation frequencies do depend strongly on the overlap of the two species, as could be inferred from Refs. [11–13]. In the process, we verified numerically the recent analytical single-condensate excitation frequency results in the hydrodynamic limit of Fliesser *et al.* [23]. In addition, by directly investigating the variations in the number density, we were able to identify those excitations for which the simultaneous response of both atomic species is likely to be experimentally observable.

ACKNOWLEDGMENTS

This work was supported in part by the U.S. Department of Energy, Office of Basic Energy Sciences. We acknowledge many useful discussions with J.R. Ensher, E.A. Burt, and J.L. Bohn.

[1] M. H. Anderson, J. R. Ensher, M. R. Matthews, C. E. Wieman, and E. A. Cornell, Science **269**, 198 (1995).
[2] C. C. Bradley, C. A. Sackett, J. J. Tollett, and R. G. Hulet, Phys. Rev. Lett. **75**, 1687 (1995); R. G. Hulet, C. C. Bradley, C. A. Sackett, and J. J. Tollett, Bull. Am. Phys. Soc. **41**, 1130 (1996).
[3] K. B. Davis, M. O. Mewes, M. R. Andrews, N. J. van Druten, D. D. Durfee, D. M. Kim, and W. Ketterle, Phys. Rev. Lett. **75**, 3969 (1995).
[4] C. J. Myatt, E. A. Burt, R. W. Ghrist, E. A. Cornell, and C. E. Wieman, Phys. Rev. Lett. **78**, 586 (1997).
[5] D. S. Jin, J. R. Ensher, M. R. Matthews, C. E. Wieman, and E. A. Cornell, Phys. Rev. Lett. **77**, 420 (1996).
[6] M. O. Mewes, M. R. Andrews, N. J. van Druten, D. M. Kurn, D. S. Durfee, C. G. Townsend, and W. Ketterle, Phys. Rev. Lett. **77**, 988 (1996).
[7] J. R. Ensher, D. S. Jin, M. R. Matthews, C. E. Wieman, and E. A. Cornell, Phys. Rev. Lett. **77**, 4984 (1996).
[8] M. R. Andrews, C. G. Townsend, H. J. Miesner, D. S. Durfee, D. M. Kurn, and W. Ketterle, Science **275**, 637 (1997).
[9] C. C. Bradley, C. A. Sackett, and R. G. Hulet, Phys. Rev. Lett. **78**, 985 (1997).
[10] H. Pu and N. P. Bigelow, Bull. Am. Phys. Soc. **42**, 1096 (1997).
[11] T. L. Ho and V. B. Shenoy, Phys. Rev. Lett. **77**, 3276 (1996).
[12] R. Graham and D. Walls, e-print cond-mat/9611111.
[13] B. D. Esry, C. H. Greene, J. P. Burke, Jr., and J. L. Bohn, Phys. Rev. Lett. **78**, 3594 (1997).
[14] B. D. Esry, Phys. Rev. A **55**, 1147 (1997).
[15] K. Huang and C. N. Yang, Phys. Rev. **105**, 767 (1957).
[16] N. P. Proukakis, K. Burnett, and H. T. C. Stoof, e-print cond-mat/9703199.
[17] M. Edwards, P. A. Ruprecht, K. Burnett, R. J. Dodd, and C. W. Clark, Phys. Rev. Lett. **77**, 1671 (1996).
[18] A. Mann, Phys. Rev. A **4**, 750 (1971).
[19] J. P. Burke, Jr., J. L. Bohn, B. D. Esry, and C. H. Greene, Phys. Rev. A **55**, R2519 (1997).
[20] P. S. Julienne, F. H. Mies, E. Tiesinga, and C. J. Williams, Phys. Rev. Lett. **78**, 1880 (1997).
[21] S. J. J. M. F. Kokkelmans, H. M. J. M. Boesten, and B. J. Verhaar, Phys. Rev. A **55**, 636 (1997).
[22] S. Stringari, Phys. Rev. Lett. **77**, 2360 (1996).
[23] M. Fliesser, A. Csordás, P. Szépfalusy, and R. Graham, e-print cond-mat/9706002.
[24] J. L. Bohn and P. S. Julienne, Phys. Rev. A **56**, 1486 (1997).
[25] J. M. Vogels, C. C. Tsai, R. S. Freeland, S. J. J. M. F. Kokkelmans, B. J. Verhaar, and D. J. Heinzen, Phys. Rev. A **56**, R1067 (1997).
[26] J. P. Burke Jr., J. L. Bohn, B. D. Esry, and C. H. Greene (unpublished).
[27] A. deShalit and H. Feshbach, *Theoretical Nuclear Physics Volume 1: Nuclear Structure* (Wiley, New York, 1974).
[28] D. J. Thouless, *The Quantum Mechanics of Many-Body Systems* (Academic, New York, 1972).
[29] R. J. Dodd, M. Edwards, C. J. Williams, C. W. Clark, M. J. Holland, P. A. Ruprecht, and K. Burnett, Phys. Rev. A **54**, 661 (1996).
[30] J. L. Bohn, B. D. Esry, and C. H. Greene (unpublished).